Acta Astronautica 246 (2026) 717–733

Contents lists available at ScienceDirect

Acta Astronautica

journal homepage: www.elsevier.com/locate/actaastro

Research paper

Satellite launch traffic forecast based on the global Gross Domestic Product and constellation plans

Wiebke Retagne *, Camilla Colombo

Politecnico di Milano, Department of Aerospace Science and Technology, Via la Masa 34, Milano, 20156, Italy

ARTICLE INFO

Keywords:
Time-series forecasting
ARIMA
LSTM
Launch traffic
Machine learning in space
Space economy
Constellation launches
Exogenous data

ABSTRACT

Satellite launch traffic is an important input into space debris evolutionary models. Slight variations in launch traffic can have a large impact on the space landscape as a whole, since the number of satellites in orbit directly influences collision risk. In recent years the trend has been going towards employing satellite constellations such as Starlink. Information about planned constellations is publicly available and is used in this work to predict the future launch traffic. The 8 largest constellations launched so far and 35 future planned constellations are considered. For non-constellation launches instead economic time series methods such as the Seasonal Auto Regressive Integrated Moving Average model and the Long Short-Term Memory model are employed. It is shown that the Seasonal Auto Regressive Integrated Moving Average model clearly outperforms the Long Short-Term Memory model. The increase in launch traffic does not happen in a vacuum and is greatly influenced by outside factors such as the general economy. As a novelty, this work also includes the global Gross Domestic Product as an economic influence on the satellite launch traffic. Including the Gross Domestic Product as an influence in the launch traffic improved predictions by 53%. Combining both constellations and non-constellation, the yearly number of objects launched could reach up to 12,000. This huge number demonstrates the need for guidelines for future launches and mitigation measures.

1. Introduction

Sputnik 1 marked the beginning of the space age in 1957. However, engineers of that era could not have predicted how much the space landscape would change over the course of 60 years. At the beginning access to space was restricted to government agencies, launchers were expensive and the development of missions took years. In the last 10 years instead, with the rise of New Space, the trend is going towards numerous, smaller missions. Companies like SpaceX offer affordable launches for commercial purposes and are also heavily involved in launching their own satellites. The space environment has turned into a highly complex system, with multiple stakeholders. This has an immense impact on factors such as astronomy, space traffic management and orbital capacity. Starlink alone made 50,000 collision avoidance maneuvers in just 6 months [1]. With the growing number of launches, the likelihood of catastrophic events leading to a chain reaction increases. Policies and mitigation measures, such as the 5-year PMD guideline, have been introduced to avoid the proliferation of space debris. These are based on projections of the future space environment. The evolution of the space environment heavily depends on the future launch traffic. The ability to forecast future launch traffic is increasingly important, as the space industry continues to grow. Launches are dictated by political, economical and technological factors. This work aims to develop a realistic, comprehensive model to forecast the future number of objects launched under the influence of economic effects. For this, the future constellation launches, as stated on the NewSpace Index website [2], are analysed and a possible launch plan based on a success rate is developed. For non-constellation launches economic influence, mainly the Gross-Domestic-Product (GDP) and historical data is considered to forecast the future number of objects launched .

A variety of methods for launch traffic modelling has been developed in literature. Klinkrad (2006) [3] differentiates between two types of future traffic model: the steady-state model and the mission model. The steady state model assumes that future launch traffic will show the same trends as historical activity. The mission model instead is based on estimates of the future use of space, such as new trends in technology. In most space debris models, such as EVOLVE [4], DAMAGE [5], LEGEND [6], and MEDEE [7] a steady-state model is used. The launch traffic of the last 5–8 years is used to create a "business-as-usual" scenario. This launch traffic is then simply repeated. This provides a good first estimate for sensitivity analysis, but does not accurately capture the evolving space landscape. Furthermore,

* Corresponding author.
E-mail addresses: wiebke.retagne@polimi.it (W. Retagne), camilla.colombo@polimi.it (C. Colombo).

https://doi.org/10.1016/j.actaastro.2026.04.046
Received 29 September 2025; Received in revised form 20 March 2026; Accepted 19 April 2026
Available online 25 April 2026

constellation and non-constellation launches are treated in the same manner through repeating the launch traffic, even though their trends and evolution are very different. Klinkrad recommends to combine the steady-state model with a mission model. This is especially useful when treating non-constellation and constellation launches separately. Non-constellation launches can be determined through historical data and constellations can be added based on a model. One approach is to fit the historical launch traffic, as is done in [8,9]. The fitting parameters are varied depending on a qualitative assumption of the future launch rate. In both cases constellations are treated separately and only a handful of constellations are included such as OneWeb or Starlink. An effort to develop reference scenarios for space debris environment modelling is presented in [10]. The authors repeat non-constellation launch traffic in a 10 year cycle multiplied by a factor depending for the demand for launch traffic. The constellation launches are based on regulatory filings for large constellations. The influence and integration of economic effects on the space debris environment has been studied for example by Wiedemann (2004) [11] and Rao and Letizia (2021) [12]. Wiedemann presents a cost and benefit analysis for space debris mitigation measures. The presented model compares a business-as-usual launch scenario with scenarios considering different types of mitigation measures to investigate the cost. In Rao and Letizia (2021) [12] an effort to combine behavioural models of orbit use with physical models of orbital environment evolution is presented. An econometric model of satellite operator's launch decisions is developed and combined with a Particle-in-a-Box debris model. The operators are divided by commercial, civil government and defence types. In the first step the number of satellites for each operator category based on economic factors and the state of the orbital environment is assessed. Then these launches are distributed across different orbital shells under the consideration of orbit characteristics, collision risk and access costs. In this way the operator's response in terms of future launch behaviour to scenarios such as fragmentation events, changing access costs or policy introduction can be quantified.

The present work builds on this approach within the GREEN SPECIES project, funded by the European Research Council through a Consolidator Grant . The GREEN SPECIES project proposes an interdisciplinary framework for the control of space debris, with the goal of identifying optimal strategies under different target scenarios [13]. Specifically, the present work develops a launch traffic forecast based on economic influences and future constellation plans. The constellation launches are modelled based on the future planned constellations according to the NewSpace Index website [2]. Likely, not all companies will actually achieve their plans, so a success rate based on historical data is calculated. The launch rate of the constellations is determined based on the planned size of the constellation and its target year of completion. For the non-constellation launches instead, time series methods are utilised. These predict future variables based on a historical input. Time series forecasting has numerous applications, ranging from forecasting the fashion industry [14], to economy [15] and forecasting the spread of diseases such as Monkeypox [16]. In space applications it can be used for example for space weather forecasting [17], telemetry health monitoring [18] or space traffic management [19]. A more in detail description of space domain applications can be found in Section 2.1. Despite this wide range of time series forecasting methods across different domains, the application of time series methods to predict future objects launched has not been studied in detail. This approach was first presented in Retagne et al. (2025) [20] and is extended in the current work. For the historical launch data information from ESA DISCOS (Database and Information System Characterising Objects in Space) [21] is used. This is a single-source reference for launch information, object registration details, launch vehicle descriptions, as well as spacecraft information for all trackable, unclassified objects. Spacecraft launch traffic and economic developments are deeply connected. Similarly to the number of objects launched, venture capital investment in space and defence reached a new historic high in 2024 in Europe [22]. As a novelty, this work focuses on extending the models with economic data as an additional input. In particular, the global Gross Domestic Product (GDP) is used. This method requires to develop also a forecast for the GDP, since this is used as an input to predict the future number of objects launched. As time series models, the Seasonal Autoregressive Integrated Moving Average model (SARIMA) [23] and the Long Short Term memory (LSTM) [24] models are implemented with both no economic data and economic data to quantify the influence of the GDP data on the launch prediction. The models are validated against test data and then used to predict future launch values. Finally, the constellation launches and non-constellation launches are combined to demonstrate what the future launch schedule could look like. The combination of time series methods with economic indicators and the planned future constellations advance this model from reference scenarios to an actual realistic forecast of future launches. This paper is organised as follows: in Section 2 the theoretical background for the modelling techniques are explained. Then, in Section 3 the future constellation launches are determined based on available constellation plans. In Section 4 the non-constellation launches are forecasted using the aforementioned time series techniques with the GDP as an additional factor. The combination of both constellation and non-constellation launches is presented in Section 5. Finally, the results are presented and discussed in Section 6.

2. Methodology

In this section methodology and the theoretical background for the modelling techniques are explained.

2.1. Time series forecasting

Time series forecasting is the process of using historical observations to predict future values. A comprehensive overview of the different methods can be found in [25]. The historical data is used to develop a model that captures the underlying trends and patterns in the data. A time series is characterised by its trend, seasonality and noise. These trends and patterns can then be used to predict future values and help in decision making processes. In the space domain, time series techniques have been adopted broadly. In Chen et al. (2019) [18] a combination of LSTM and ARIMA is used to predict the time series data of a meteorological satellite telemetry parameter. Satellite telemetry generates a large amount of data, making it perfect for the application of time series methods. Besides using it to predict the health of the satellite, the telemetry can also be used to analyse Earth observation data [26]. In Picoli et al. (2018) [26] a support vector machine model is used to produce land use and land cover classification over large areas in Brazil from 2001 to 2016. An application directly in the space sustainability domain is presented in Stevenson et al. (2023) [19]. Here, self-supervised machine learning is used for orbit modelling and applied to space traffic management. Similarly to the launch traffic, the space weather has to be predicted in long-term debris evolutionary models. Thaker et al. (2025) [27] provides an overview of AI approaches for space weather prediction. This study found that deep learning approaches such as LSTM provide good temporal predictions for space weather forecasting. Given these promising results for other space domain applications, in this work time series forecasting is applied to the launch traffic.

Generally, time series methods are divided into classical methods and machine learning/deep learning methods. The classical methods include statistical models such as a moving average, exponential smoothing and ARIMA (see Section 2.2) to make predictions, while the machine learning methods include neural networks, random forests and gradient boosting methods. In this work the deep learning model LSTM (see Section 2.3) is used. There are also hybrid approaches that for example use a statistical method to learn the trend and use the residuals as an input for an LSTM model. To classify the accuracy of the forecast

usually the historical data is split into a test and a training dataset. Then, metrics such as the Mean-Squared Error (MSE) are used to assess the quality of the predictions. The MSE is defined as seen in Eq. (1).

$$MSE = \frac{1}{n}\sum_{i=1}^{n}(y_i - \hat{y}_i)^2, \tag{1}$$

where n is the number of observations and y_i represents the actual value and $\hat{y}_i$ the predicted value. In this work the parameter y refers to the number of objects launched. In the following, the time series methods used in this work for launch traffic forecasting are explained in more detail.

2.2. SARIMAX

The ARIMA model, which is based on Box and Jenkins [28] and its extensions have been popular in time series forecasting for a long time due to its ease of use and reliability. In this work the SARIMA and SARIMAX models [23] are used. The acronyms describe the key elements of the model:

- **S**(s) Seasonality: Seasonal effects such as weather or holidays
- **AR**(p) Autoregression: Regression model. A regression model relates two or more variables by fitting a function to the observed data. In the case of the ARIMA model the function is linear. And the dependent variables are the past values of the time series itself.
- **I**(d) Integrated: Differencing to make time series stationary. Differencing describes the subtraction of the previous time step from the current value.
- **MA**(q) Moving Average: It is a linear regression model of the current value against observed error terms.
- **X** Exogenous variable: An outside variable that influences the evolution of the time series

The autoregression term models the relationship between a past observable y_{t-1} and the current state y_t. The t represents the current time step of the time series. Mathematically it can be defined as seen in Eq. (2).

$$y_t = c + \sum_{i=1}^{p}\phi_i y_{t-i} + \epsilon_t. \tag{2}$$

The order p describes how many past terms y_{t-i} are taken into consideration when estimating the current term y_t. c is a constant term. ϕ_i is the corresponding coefficient, which weights each lagged observation. The error terms ϵ_t are defined as noise errors. This means that the error consists of uncorrelated random variables with a mean of zero and a constant variance. Using the backshift operator B (Eq. (3)), Eq. (2) can be rewritten to Eq. (7). The backshift operator B^i transforms the current state y_t to a past state y_i.

$$(B^i)y_t = y_{t-i}. \tag{3}$$

Eq. (2) can be rewritten by substituting $y_{t-i} = B^i y_t$.

$$y_t = c + \sum_{i=1}^{p}(\phi_i B^i)y_t + \epsilon_t. \tag{4}$$

$$\left(1 - \sum_{i=1}^{p}(\phi_i B^i)\right)y_t = c + \epsilon_t \tag{5}$$

Through defining the AR polynomial operator $\phi(B)$ with the standard sign convention, as seen in Eq. (6).

$$\phi(B) = 1 - \phi_1 B - \phi_2 B^2 - \cdots - \phi_p B^p \tag{6}$$

The AR model can be rewritten as seen in Eq. (7).

$$\phi(B)y_t = c + \epsilon_t \tag{7}$$

This is then combined with a moving average model, which takes the previous error terms ϵ_{t-j} into account. The parameter q defines the number of error terms taken into account. Specifically, it is a linear regression model of the current value against previously observed error terms, with the addition of a constant c. The θ_j are the coefficients representing the moving average part. It is defined in Eq. (8).

$$y_t = \mu + \epsilon_t + \sum_{j=1}^{q}\theta_j \epsilon_{t-j}, \tag{8}$$

where μ is the mean of the series. Similarly to before, the backshift operator B can be used on the error terms to rewrite Eq. (8) to Eq. (11) with the use of the MA polynomial operator $\theta(B)$.

$$(B^j)\epsilon_t = \epsilon_{t-j} \tag{9}$$

$$\theta(B) = 1 + \theta_1 B + \theta_2 B^2 + \cdots + \theta_q B^q \tag{10}$$

$$y_t = \mu + \theta(B)\epsilon_t \tag{11}$$

The leading 1 in $\theta(B)$ corresponds to the explicit ϵ_t term in Eq. (8). Combining Eq. (7) and (11) yields the ARMA model as seen in Eq. (12).

$$\phi(B)y_t = c^* + \theta(B)\epsilon_t, \tag{12}$$

where c^* is a constant that combines the constants c and μ from the AR and the MA model in one single constant. This model can only be applied to stationary time series, where the statistical properties such as the mean and variance do not change over time. The ARIMA model is an extension of this, which transforms non-stationary time series models into stationary ones through a process called differencing. The value of a time series at a previous time step is subtracted from the current value. The order of differencing is denoted by the number of primes $'$. An example of first order differencing can be seen in Eq. (13)

$$y'_t = y_t - y_{t-1} = (1 - B)y_t. \tag{13}$$

This differencing is applied to the time series prior to then using the ARMA model equation (Eq. (12)) on the new, differenced time series values. This can be seen in Eq. (14).

$$\Delta^d y_t = (1 - B)^d y_t, \tag{14}$$

where $\Delta^d y_t$ is the dth differenced time series and B is the backshift operator as defined in Eq. (3). In summary, the ARIMA model can be characterised by the number of lags p, the number of error terms q and the number of differences d, depending on the time series properties. The equation can be written as shown in Eq. (15).

$$(\phi(B)\cdot\Delta^d)y_t = c^* + \theta(B)\epsilon_t. \tag{15}$$

Many time series are influenced by seasonal effects such as weather or certain holidays. To include this seasonality into the ARIMA model it can be extended through a multiplicative model. In the seasonal time series, the forecast is now influenced by the last observed value from the same season (for example the same month of the previous year). As with the ARIMA model there are the parameters (P, Q, D) which describe the seasonal lags, seasonal moving average and the seasonal differencing. There is one additional parameter s, which describes the length of the cycle. For example, if the data is yearly and the seasonality appears once every 4 years the parameter would be $s = 4$. The seasonal AR and MA polynomial operators are defined analogously to their non-seasonal counterparts, using B^s lags. This is defined in Eq. (16) and (17).

$$\Phi_P(B^s) = 1 - \Phi_1 B^s - \Phi_2 B^{2s} - \cdots - \Phi_P B^{Ps}, \tag{16}$$

$$\Theta_Q(B^s) = 1 + \Theta_1 B^s + \Theta_2 B^{2s} + \cdots + \Theta_Q B^{Qs}. \tag{17}$$

The seasonal differencing operator is defined in Eq. (18).

$$\Delta_s^D y_t = (1 - B^s)^D y_t. \tag{18}$$

The full SARIMA model is then described by $(P, Q, D, s)\times(p, q, d)$ [23]. The effect of the seasonality is applied by multiplying the seasonal operators to the time series.

$$\left(\Phi_P(B^s)\cdot\phi(B)\cdot\Delta^d\cdot\Delta_s^D\right)y_t \tag{19}$$

$$= c^* + (\theta(B)\cdot\Theta_Q(B^s))\epsilon_t. \tag{20}$$

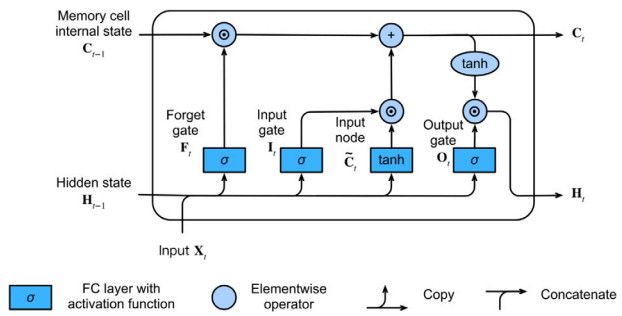

Fig. 1. The schematic of an LSTM unit. It is characterised by a memory state which transports information across the unit and three different gates. The forget, input and output gate. The gates regulate the flow of information in and out of the cell.
Source: Figure taken from [29].

The operators $\phi(B)$, $\theta(B)$ and Δ^d refer to the previously defined (Eq. (6), Eq. (10) and (14)) ARIMA operators. In addition to the historic time series data external predictors can be considered in the SARIMAX model [23]. These are external variables that might have an impact on the evolution of the original time series. These terms are simply added to the SARIMA equations.

$$(\Phi_P(B_s^P)\cdot\phi_p(B^p)\cdot\Delta^d\cdot\Delta_s^D)y_t \tag{21}$$

$$=c^*+(\theta_q(B^q)\cdot\Theta_Q(B_s^Q))\epsilon_t+\beta^\top X_t. \tag{22}$$

with X_t the vector of the exogenous variables and β the coefficients for X_t.

2.3. Machine learning

While the ARIMA model is popular it has some limitations when modelling non-linear relationships. Here, deep learning methods can come into play. The nature of the sequential data in time series make them well suited for Recurrent Neural Networks (RNNs) due to their ability to capture nonlinear short-term time dependencies. Long Short-Term Memory (LSTM) networks are an extension of RNNs that deal with the vanishing gradient problem. They were first introduced in 1997 by Hochreiter and Schmidhuber [24] and have since found many applications in time series, natural language processing or economics and finance. An input x is given into a hidden layer with LSTM units. The LSTM unit consists of one cell state and three gates: the input gate, the forget gate and the output gate. The cell state acts as a memory and carries the relevant information across the time steps. The flow of information is controlled by the different gates. Each unit is characterised by an activation function. The data flow is depicted in Fig. 1.

In the following the gates of the LSTM unit are described in more detail [29].

Forget gate

The forget gate F_t takes care of removing the information that is no longer useful from the cell state. It receives two inputs: X_t, the input at a given time and H_{t-1} the previous cell output. These inputs are then multiplied with weight matrices W_f followed by the addition of a bias b_f. The result is then passed through a sigmoid activation function σ. This returns a value in the range between 0 and 1. If the output is 0 the information is thrown away, if the output is 1 the information is kept for future use. Intermediate values result in a proportional amount of information being passed through. The final equation of the forget gate is described in Eq. (23).

$$F_t=\sigma(W_f\cdot[H_{t-1},X_t]+b_f). \tag{23}$$

Input gate

The input gate I_t is responsible for adding useful information to the cell state. The information is regulated again through a sigmoid function σ and the values are filtered similar to the ones in the forget gate by multiplication with weight matrices W_i and the addition of a bias b_i. A vector input $\hat{C}_t$ is created by using a tanh function with outputs from −1 to +1 which contains all possible values from h_{t-1} and x_t. Then the regulated values are multiplied with the vector to obtain the information that is useful to be contained in the cell state C_t.

$$I_t=\sigma(W_i\cdot[H_{t-1},X_t]+b_i) \tag{24}$$

$$\tilde{C}_t=\tanh(W_c\cdot[H_{t-1},X_t]+b_c) \tag{25}$$

$$C_t=F_t\cdot C_{t-1}+I_t\cdot\tilde{C}_t. \tag{26}$$

Output gate

The output gate O_t extracts the useful information from the current cell state. The information is regulated with a sigmoid function σ and the values are filtered using the inputs H_{t-1} and X_t and by multiplication with weight matrices W_o and the addition of a bias b_o. The regulated values and the vector $\tanh(C_t)$ are multiplied and send as output H_t to the next cell.

$$O_t=\sigma(W_o\cdot[H_{t-1},X_t]+b_o). \tag{27}$$

$$H_t=O_t\cdot\tanh(C_t). \tag{28}$$

This describes the architecture of the LSTM memory cells. The weights of the LSTM model are adjusted iteratively during training via back propagation and through minimising a loss function. Over many iterations the weights converge to capture the underlying temporal dynamics.

3. Constellations

The constellations and non-constellation objects follow a very different trend. Especially with the rise of New Space, the number of constellation satellites in the last 5 years has increased significantly. While at the beginning of spaceflight the objects launched consisted of singular missions, now the trend has shifted and more and more constellations are being launched. Due to this reason in the launch forecast they are treated separately. Specifically, constellations are filtered out of the historical DISCOS data [21] that is used to predict the future number of objects launched with SARIMAX/ML. Then, for the filtered out constellations their future launch plans are documented. Here, two factors are considered: constellations that have already started launching and future constellation plans according to the NewSpace Index website [2]. This paper adopts the same formalism as the NewSpace Index website: a constellation is made up of three or more satellites. As of July 2025, the NewSpace Index website lists 432 constellations. These include failed/cancelled constellations and those that have an unknown status. For simplicity here these three categories have been combined into one “failed” constellations category. Additionally, the website includes constellations that have already started launching and those that have been announced for the future. Starting from 2025, there are 93 completely new constellations planned. Of these, 66 have stated their planned number of satellites. Of the historical constellations, a total of 339 constellations have been announced. Of these, 160 have then failed for different reasons or have an unknown status. This corresponds to a success rate of 53% (160/339). To note is that the NewSpace website treats all Starlink batch launches as separate constellations. One of the future planned constellations is a Starlink V3 launch. To avoid counting these planned satellites in both the launched constellations and the future constellations, this specific launch is considered as an active constellation that is “yet to launch”, reducing the number of future planned constellations from 66 to 65. Analysing this in terms of number of satellites Fig. 2(b) is useful. The following can be observed: of the constellations that started launching, 12,519 satellites have already been launched. For these constellations, 31,506 satellites are yet to be launched, not considering replenishment of the out of service satellites. In the future, for the 65 constellations

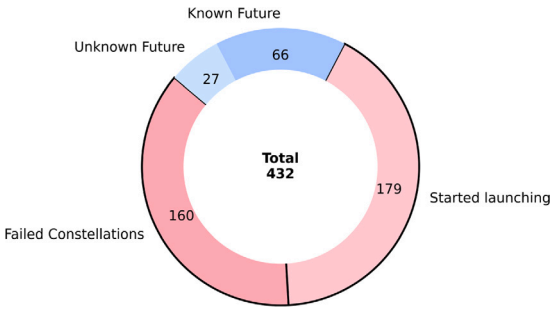

(a) All 432 constellations listed on the NewSpace Index website [2] broken down by their status. There are 93 new constellations planned in the future, with 66 of them giving detailed plans. Of the 339 historical constellations almost half have stopped launching satellites.

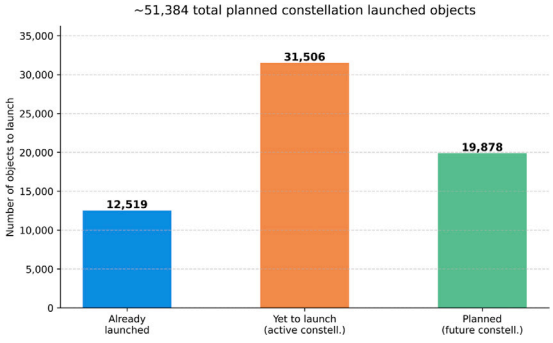

(b) The constellations listed on the NewSpace Index website [2] split by number of satellites. For the constellations that have already started launching, there are 31,056 satellites still to be launched. Additionally, 19,876 future objects are planned. Replenishment is not considered.

Fig. 2. Overview of constellation data from the NewSpace Index website [2].

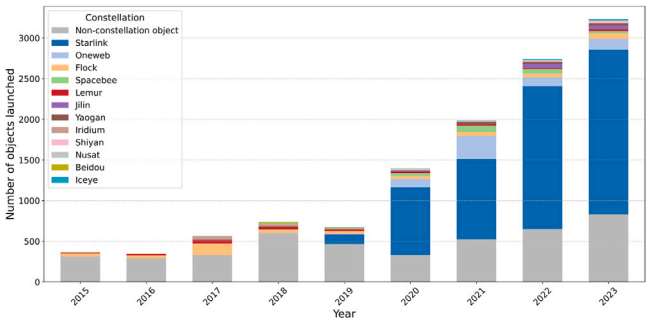

Fig. 3. The historical launch data divided by the largest satellite constellations since 2015 based on DISCOS data [21]. The increase in launches is largely due to the Starlink constellation.

Table 1
The 15 largest satellite constellations since 2015 and the added Guo Wang constellation and their launch plans. This data includes constellations that have already finished launching. 8 constellations still need to be completed. These are marked in italic. For the military constellations the final number of satellites is not public. The ones with the most planned satellites (Starlink, Qianfan, Guo Wang) are all related to internet access.

Constellation	Info	Launched/Planned	First/Finish launch
Starlink	Internet access	7665/12,000	2019/2029
OneWeb	Internet access	656/756	2019/2027
Flock	Earth observation	514/180	2015/2020
SpaceBee	Communications	201/150	2018/2025
Lemur	Earth observation	181/150	2015/2020
Jilin	Earth observation	138/300	2015/2030
Yaogan	Chinese military	129/?	2015/2030
Starshield	US military	104/?	2024/?
Iridium	Communications	80/66	2017/2022
Shiyan	Classified Chinese	61/?	2017/?
Qianfan	Internet access	54/15,000	2024/2034
Nusat	Earth observation	47/50	2016/2021
Beidou	Navigation	44/45	2015/2020
Sitro	Earth observation	44/70	2024/2029
Iceye	Earth observation	40/70	2018/2026
Guo Wang	Internet access	29/12,992	2024/2034

that have stated their planned number, an addition of 19,878 satellites is planned. As a result, theoretically there are a total of more than 50,000 planned satellite launches for constellations alone, not even considering replenishment. This is the worst case scenario (or best case if you are a constellation operator), but taking the success rate of 53% into account it is likely that not all of these launches will actually happen. In the following a possible scenario for the future launches of constellations is determined.

3.1. The 15 largest constellations since 2015

Firstly, the constellations that have already started launching are investigated. To properly filter out the constellations from the DISCOS data and to separate constellations and non-constellation launches it is necessary to match the data from the NewSpace Index website to the DISCOS data. The DISCOS data has no information about whether or not the object is a constellation object. As a first filter, only Payload objects are considered. Furthermore, the database does provide a "Name" column. This column is used to look for objects with the same words inside the name. Common words such as "Satellite, Star, Space" need to be disregarded. Then, the common words are sorted by their number of occurrence. This is directly proportional to the already launched satellites. In this way, the 15 largest satellite constellations since 2015 can be found. The term "largest" referring to the number of already launched satellites. If an object contains the words in the common word list, it is assigned as a constellation, otherwise it is a non-constellation object. The number of historical launches since 2015 divided into non-constellation objects and these selected constellations can be seen in Fig. 3.

Clearly, Starlink has the largest contribution to the number of objects launched in the last 10 years. In general, the number of constellation objects far exceed those of non-constellations since 2020. For these constellations the number of launched satellites and the planned number of active satellites has been collected again based on the NewSpace Index website [2]. This overview can be seen in Table 1. In the later course of this work, Table 1 also serves to filter the DISCOS data of constellation objects: this allows the data to be used as an input for the models to determine future non-constellation objects (see Section 4.1). Therefore, Table 1 includes constellations that have finished their launch plans. For the Yaogan, Starshield and Shiyan constellations there is no planned number of satellites available, since these are classified military missions. The largest constellations all plan to provide internet access. Just considering these constellations there are a total number of 19,173 satellites still to be launched. The main contributions are from Starlink and the Chinese Starlink competitor Qianfan. The data for the 15 already launched constellations coming from DISCOS are compared to the data for all constellations coming from NewSpace in Table 2.

Comparing this with the number (31,506) obtained by all 179 constellations that have started launching there are 12,333 satellites not accounted for when just considering the 15 largest constellations in the last 10 years. Here, the term "largest" referred to the already launched satellites. Instead now the planned number of satellites is considered

Table 2
The active constellation data coming from DISCOS and from the NewSpace website compared. This does not consider replenishment.

Number of	15 DISCOS constellations	All NewSpace constellations
Launched satellites	9958	12,519
Future satellites	19,173	31,506

for those that have already started launching. Inspecting this, there are several constellations which have had their first launch years ago but have not had an update since. For example SatRev [30] states they want to launch 1024 satellites for earth observation, but have only launched 9 satellites since 2019. According to their own statements by 2023 they wanted to have already 66 satellites in orbit. While in the NewSpace Index website these are still marked as "ongoing", it is unlikely that they will actually launch 1024 satellites by 2026. Therefore, this specific example and those like it are discarded for the future launch traffic. Disregarding these reduces the number of planned satellites by 5000, leaving (12333-5000) = 7333 satellites unaccounted for. To represent these for the future launches there is one more large constellation added which was not captured by the original search for the largest constellations in DISCOS, since it has just started launching satellites in 2024. This is the Guo Wang, Xingwang constellation, with a total of 12,992 satellites planned, of which 29 have already launched. The final overview can be seen in Table 1. If no information is available on the planned number of satellites the current number of satellites is used. Since these constellations have launched a significant number of satellites already, all are assumed to reach full completion with no further failures.

3.2. Future constellations

For the future planned constellations only the 66 constellations that have stated their planned launch number are considered. As already mentioned, the NewSpace website lists Starlink constellation launches as separate constellations. One of the future planned constellations is a Starlink constellation, instead of including it here, it will be treated as an "already launched" constellation. This reduces the number of future planned constellations from 66 to 65. Furthermore, the success rate of 53% of the already launched constellations is applied to future constellations. This reduces the number from 65 to 34 constellations (65 ·0,53 = 34) future constellations. Depending on which 34 constellations are selected the future launch traffic changes significantly. The subset of the 34 constellations should have the same properties as the original distribution. As stated previously, 19,878 satellites are planned to be launched. Notably, 10,000 of those satellites come from one single constellation alone: the Hongqing Technology constellation [31]. The selected subset is very sensitive to whether the Hongqing constellation is included or not. This represents a source of uncertainty in the future constellation launch traffic. In the following, the impact of Hongqing is reported independently. Both the inclusion and exclusion of the Hongqing constellation is investigated. The Hongqing constellation is excluded from the calculations of the statistical properties when choosing the sub sample. In particular the mean and the median of both datasets are compared. Furthermore, it is useful to separate the constellations into categories based on their planned number of satellites and sample these categories separately. In this way, the distribution of constellation categories is preserved. The dataset is split into four equal parts using quartiles. The Q1 quartile (25th percentile) marks the value below which 25% of constellations fall, the median (50th percentile) marks the midpoint, and the Q3 quartile (75th percentile) marks the value below which 75% of constellations fall. These three points divide the data into four equally-sized groups. From each group, 53% of constellations are sampled, until the target of 34 constellations is reached. To evaluate whether the sampled dataset preserves the statistical properties of the original, the Interquartile Range (IQR) is used. The IQR is the difference between Q3 and Q1, and describes the spread of the middle 50% of the data. It is robust to outliers, making it a more reliable measure than the mean or standard deviation for skewed distributions like this one. Comparing Q1, the median, Q3, and the IQR between the dataset of 64 constellations (without the Hongqing constellation) and the sample of 34 confirms the statistical similarity between the two. The results are summarised in Table 3 and displayed in Fig. 4.

Table 3
The statistical parameters for both the full dataset of the 64 planned constellations and the sub-sample of 34 planned constellations.

Parameters	Full (64)	Sample (34)
Mean	154	145
Median	24	24
Q1	10	8
Q3	100	88
IQR	90	80
Planned satellites	9878	4935

In Fig. 4 it can be seen that most constellations still report a relatively low number of planned satellites. This is also evident in the median value of 24 per constellation. Between the original dataset and the sample dataset there is good statistical similarity. The distributions were plotted both in linear and in log scale. Due to the skewedness of the distributions the log scale allows for a better visual demonstration of the statistical parameters. The effect of the Hongqing constellation is discussed later on in Fig. 6. The full list of the 65 constellations that have stated their plans, with the subset of 34 constellations selected indicated in purple can be found in the appendix.

3.3. Replenishment and launch rate

For both the constellations that have already started launching and the newly planned constellations the launch rate and possible replenishment needs to be considered. For some constellations the companies have made statements about the planned completion year of the constellation. For example, OneWeb published they want to launch 100 more satellites by 2026 [32]. If no information is available the completion year is based on the size of the constellation. It is calculated as seen in Eq. (29).

$$T = \begin{cases} FL + 5 & \text{if } P \leq 5000 \\ FL + 8 & \text{if } 5000 < P < 10000 \\ FL + 10 & \text{if } P \geq 10000 \end{cases} \tag{29}$$

where T: the target year of completion of the constellation, FL: the year of the first launch and P: the number of planned satellites. The target year T is then used to determine the number of launched satellites L for each year. An equal spacing is assumed. This equation was derived by empirically investigating past times needed to finish constellations and by looking at company statements. If the constellation is smaller, a faster completion can be assumed. The launch rate per year is then calculated according to Eq. (30).

$$L = \frac{P - S(2025)}{T - 2025 + 1} \text{ number of objects/year}, \tag{30}$$

where, S: the number of satellites already launched in 2025 and P: the number of planned satellites. The +1 is added in the denominator because the launches for the year 2025 are also predicted. This assumes that the same number of objects each year is launched. In reality, a company might launch 100 objects in one year and only 20 the next. Since for long term debris simulations the total number of objects launched is more important than the actual number per year, this is used as an approximation. After the full capacity is achieved the constellation is only replenished after the respective satellites have reached their end of life. For each satellite a 5 year life-span is assumed. This is a common replenishment duration for large constellations such as Starlink or OneWeb due to their low orbit. After these 5 years a new

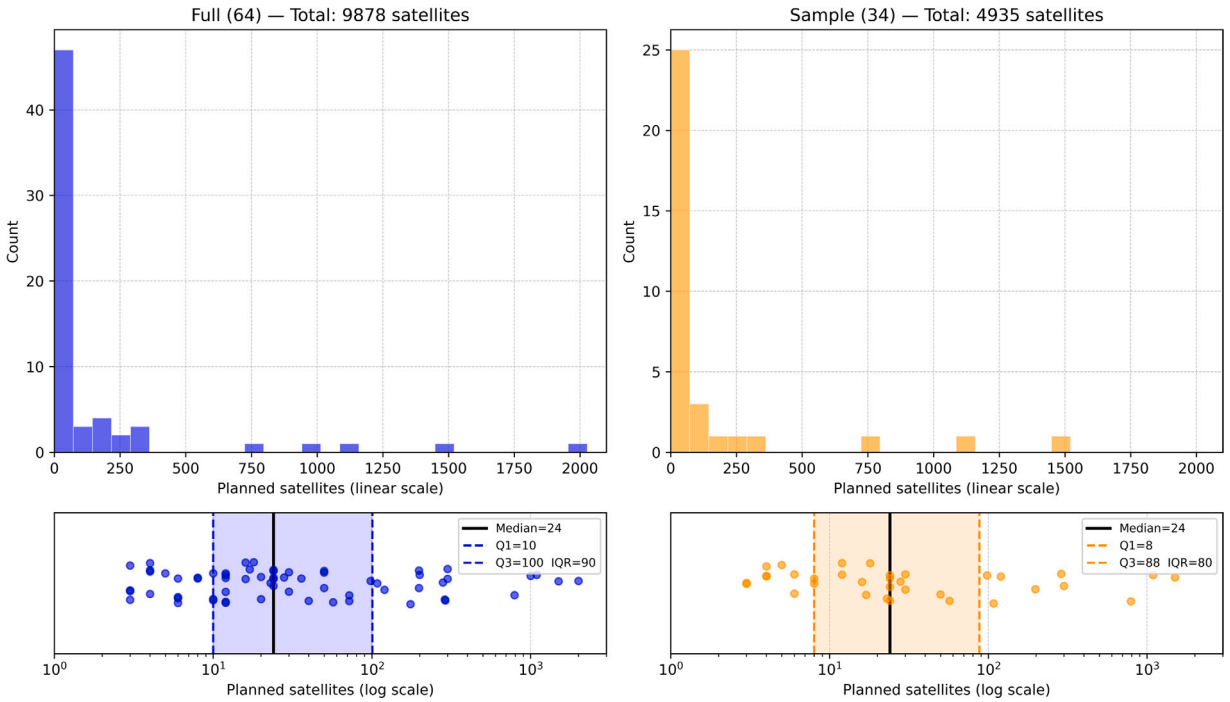

Fig. 4. The distribution of the future planned constellations, excluding the Hongqing constellation, and the subset selected shown both in the original linear scale and in log scale. It is likely that not all constellation plans will actually follow through, therefore a subset of 53% of constellations was selected for future analysis. This plot shows that the original and the subset have the same statistical properties.

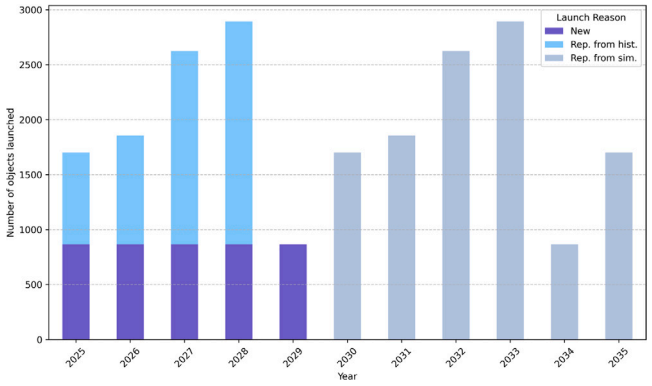

Fig. 5. Forecast of future Starlink satellites divided by launch reason. The new satellites are needed to complete the launch plans. A replenishment period of 5 years is assumed. This is broken down further into replenishment of satellites that have already launched and replenishment of the future simulated satellites. From 2030 onward the launched satellites are only due to the replenishment. (For interpretation of the references to colour in this figure legend, the reader is referred to the web version of this article.)

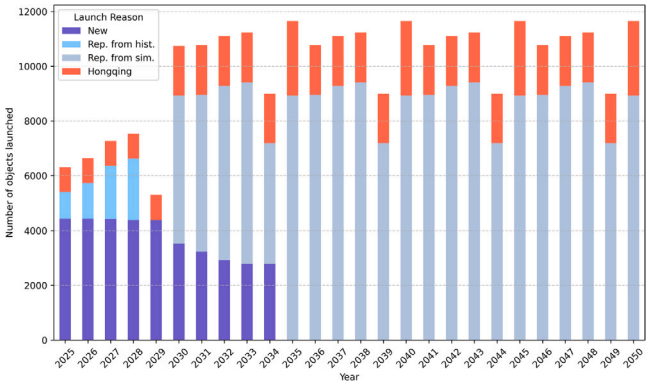

Fig. 6. Forecast of 43 future constellation satellites assuming a replenishment after 5 years. The number of launched satellites reach over 10,000 satellites per year. The bulk of these are made up of replenished satellites. In 2040 all 43 constellations have finished their original launch plans. The Hongqing constellation contributes a significant amount of satellites.

satellite is launched to replenish the constellation. This replenishment tactic also includes those satellites that have already been launched before 2025. This is demonstrated on the example of Starlink. In the year of 2025 it has 7665/12,000 planned satellites in orbit. A launch finish of 10 years after the first launch is assumed. Therefore, the annual launch rate for new satellites is

$$L = \frac{(12000 - 7665)}{(2029 - 2025 + 1)} = 867 \text{ number of objects/year.} \quad (31)$$

The forecasted number of launched satellites for the next 10 years is displayed in Fig. 5. The purple represents the annual launched satellites that Starlink has to do to reach their goal of completion by 2029. Since all satellites are assumed to have a 5 year lifespan, up until 2030 none of the newly launched satellites need to be replenished. The blue represents satellite replenishment of those that have launched before 2025. These have finished their replenishment in 2029. Consequently, a dip in the number of satellites can be observed in 2029.

The future forecast for the next 25 years including all 8 unfinished constellations from Table 1, the Hongqing constellation and the 34 future constellations can be seen in Fig. 6.

In 2035 all constellations are assumed to have finished their completion. After this point only the replenishment is a contributing factor in the number of launches, which is why the repeating pattern can be observed. The bulk of the future number of satellites is made up of the constellations that have already started launching. Depending on if there will actually be constant replenishment of the launched and planned constellations, future launch traffic will change substantially. For the Hongqing constellation (marked in red) the satellites were not

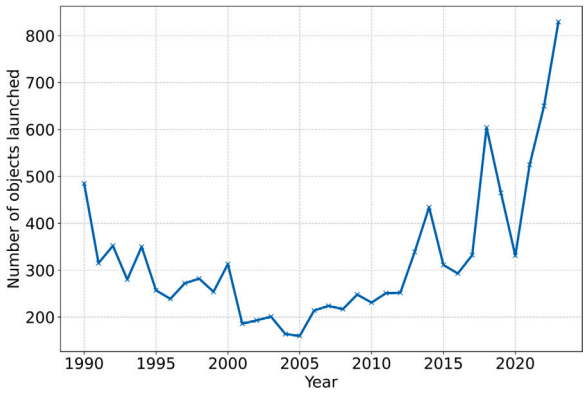

Fig. 7. Non-constellation objects aggregated yearly.

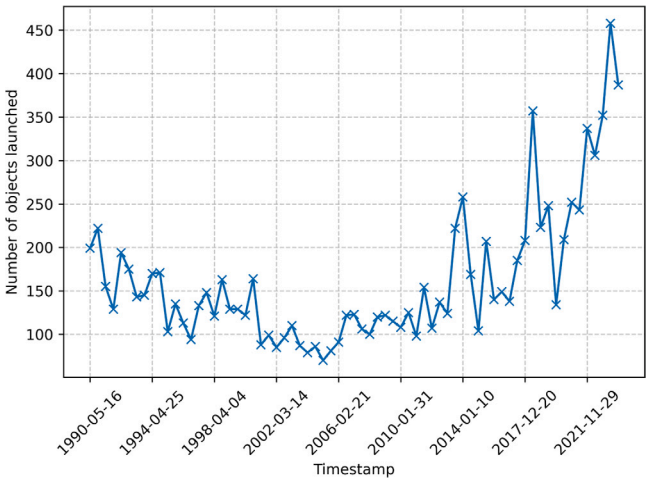

Fig. 8. Non-constellation objects aggregated every 180 days.

further split by launch reason. It is assumed to reach full size in 2035, after which the only cause for launch is replenishment. It contributes a significant number of satellites, roughly about 2000 per year. This demonstrates that the future evolution of the space environment is now largely dependent on a few single players.

4. Non-constellation launches

For the non-constellation launches the previously described time series forecasting methods ARIMA and LSTM are used. Before the methods can be applied the DISCOS data [21] and the external economic data has to be prepared to serve as an input for the models. Then, the model parameters are chosen by splitting the data into a train/test dataset. Based on this the accuracy of the model predictions can be determined using the MSE. Finally, the number of objects launched are forecasted for the next 25 years.

4.1. Data pre-processing

The DISCOS database includes not only objects launched, but also debris. Since this is not relevant for this study this is filtered out. The categories Payload, Rocket Body and Mission Related Object are considered. Furthermore, since the constellation objects are treated separately the constellations mention in Table 1 are also filtered out. The aim of this research is to predict the future number of objects launched per year. The DISCOS database has a record of every launch and its exact date. Consequently, the number of objects launched can be aggregated for any chosen timespan. For the SARIMA/SARIMAX algorithm the data is aggregated on a yearly basis. The yearly number of objects launched from 1990 to 2023 can be seen in Fig. 7.

A steady downward trend from 1990 onward can be observed. In the early 2000s the number of objects launched reach their all time low. This could possibly be connected to the turbulent times in that era which include the 9/11 terrorist attacks and the subsequent increased spending on military. After 2006 the number of objects slowly rise again. Around 2010, with introduction of the New Space sector the yearly number of objects see a stark increase. This is also when Barack Obama introduced a new policy to increase NASA funding by over $6 billion [33]. In 2020 there is a pronounced dip in the number of objects, likely due to the Covid pandemic. Interestingly, this dip is not observed when also considering constellation satellites (see Fig. 3). While government agencies and traditional space companies were heavily affected by the shutdowns, private companies such as SpaceX experienced little disruption [34]. Their autonomous operation structure, from assembly to launch, allowed them to keep up with the scheduled launches.

For the LSTM algorithm a more granular aggregation of 180 days was chosen. Aggregating the data in this way doubles the data points available for the model to learn from. This should in theory allow the LSTM model to better capture the underlying trends. The raw data, with the 15 constellations mentioned previously filtered out, is presented in Fig. 8. Most notably there is one spike in the launch data. In November 2018 104 tiny satellites called “Sprite” were launched [35]. These are a technology demonstration of cracker sized satellites.

4.2. LSTM

To validate and test the LSTM model the data is split into a test and a train dataset. Of the available data, 77% is used to train the model. In general, a split of 70%–80% is recommended. The 77% split was found to deliver the best balance between keeping the train dataset large, but still having enough of a validation dataset. The predictions of the model for this time frame are compared to the actual data. In this manner the accuracy of the model can be assessed. Producing reasonable results with the LSTM model has proved as tricky. Several tactics were employed to improve the predictions. These are listed in the following.

- Aggregate launch data every 180 days instead of yearly to increase the available data points
- Transform launch data into log space and scale it between 0 and 1
- Instead of using GDP directly as an input use the percent change
- Use a custom loss function to penalise over or under estimation and keep the forecast in a reasonable interval

Even though these changes improved the predictions, it still did not deliver reasonable results.

4.3. Economic factors

Spacecraft launch traffic is influenced by many different factors. While mankind is continuously striving towards exploring space, the governmental and public interest might vary depending on global events. When the general economy takes a hit and people are struggling, the investments in space might be put on a back burner. This paper aims to investigate the connection between the economy and objects launched. To connect the spacecraft launch traffic to economic factors there are two main things which are important: The selected data has to be correlated to the launch traffic and it needs to be easily accessible. In fact, while the original idea was to use only investments/Global Domestic Product (GDP) shares made in the space sector it was difficult to find publicly available data. Therefore, the general

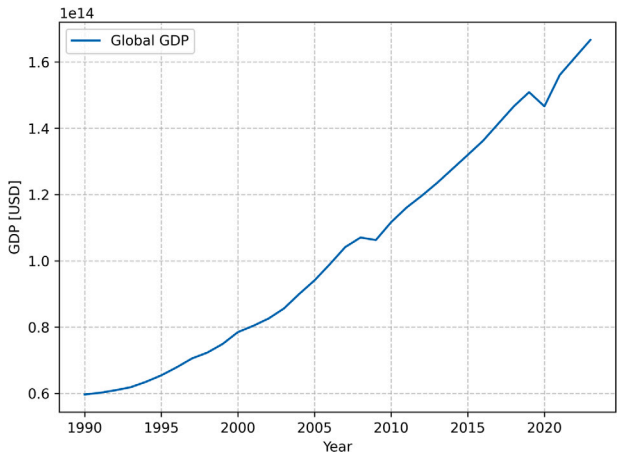

Fig. 9. The global GDP since 1990 [36]. There is a steady growth of 3% with two major outliers. The world economic crisis in 2008 and the COVID pandemic in 2020.

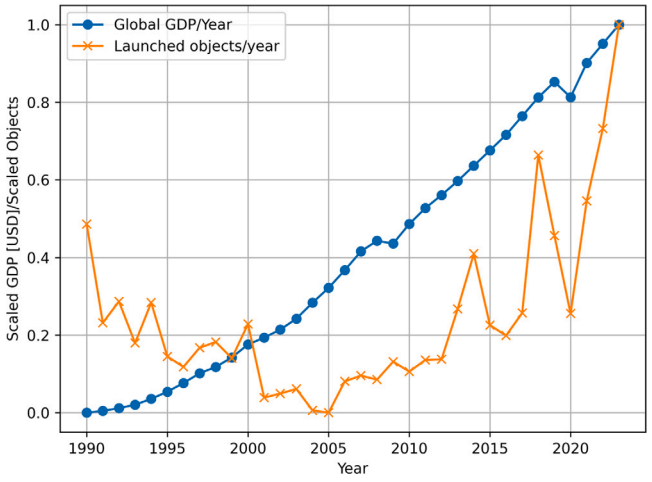

Fig. 10. Scaled non-constellation objects and scaled GDP data. The objects launched have a lot more variation compared to the global GDP. Notably, the two dips in the GDP are also reflected in the launch data. The most obvious dip is in 2020, when both the GDP and the launch data are lowered significantly.

global GDP was selected to serve as an input in the model. The data is available from 1990–2023 through the World in Data website [36]. The data can be seen in Fig. 9.

The global GDP shows a steady increase of roughly about 3%. There are two obvious drops in the data in 2008, which corresponds to the world economic crisis and 2020 due to the COVID pandemic. Budget cuts and reduced investments during this time could have an influence on the launch data.

4.3.1. Linear correlation

To affirm the correlation between the GDP and the launch traffic data the first step is to do a visual inspection. For this both the launch data and the GDP data is scaled to lay between 0 and 1. The minimum observed value of both the number of objects and the GDP is set as 0 and the highest value as 1. The minimum observed number of objects in this time period was in 2005. The lowest value for the GDP was in 1990. Then both of these can be plotted in the same plot and compared. The result is demonstrated in Fig. 10.

The global GDP shows a much more steady curve compared to the launch data. The most obvious correlation is in 2020, but also the drop around 2008 is reflected in the launch data. Besides the visual

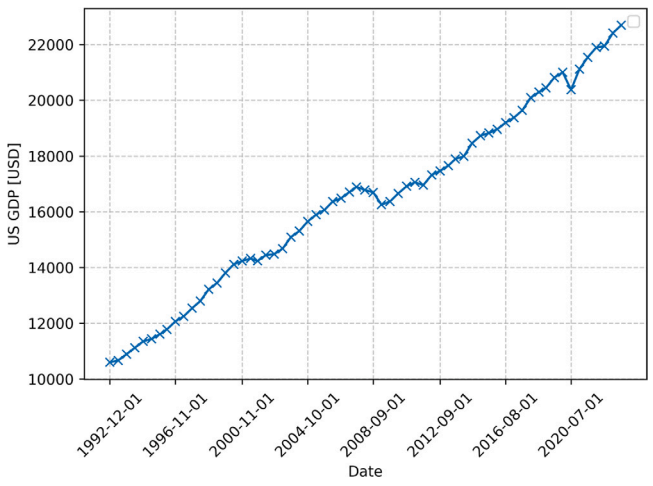

Fig. 11. The monthly GDP of the US [38]. The curve follows the global GDP very closely. There is a slight stagnation around 2001 and two obvious dips in 2008 and 2020.

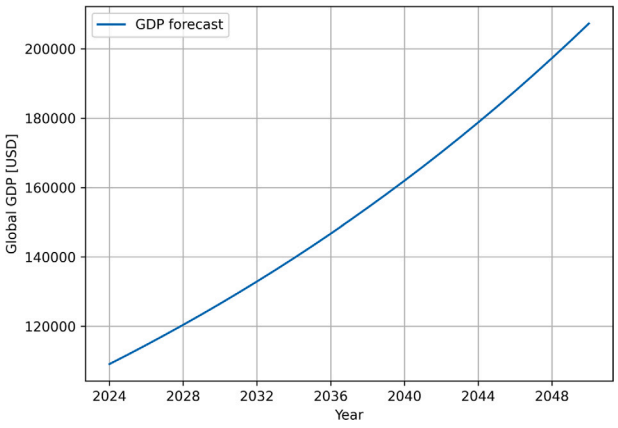

Fig. 12. The global GDP forecast assuming a constant growth of 2.5% per year. This is used as an input to predict future launch data.

inspection the Pearson Correlation Coefficient (PCC) [37] can serve as an indicator. This measures the strength of linear association between two variables. It is defined as seen in Eq. (32).

$$PCC = \begin{cases} -1: & \text{Perfect negative linear correlation} \\ 0: & \text{No correlation} \\ 1: & \text{Perfect linear correlation} \end{cases} \tag{32}$$

For the launch traffic data and the global GDP the value is $PCC = 0.57$ indicating a moderate positive linear correlation. This does not stipulate a strong correlation, but does show that the variables are connected. To have more granular GDP data available for the LSTM model instead the monthly US GDP is used. This is made available by S&P global [38]. As shown in Fig. 11 the monthly US GDP follows the trend of the global GDP closely. Similar to the yearly global GDP, the Pearson Correlation Coefficient is $PCC = 0.59$.

4.3.2. Economic forecast model

To use the global GDP not only the history but also the future forecast is needed as an input for the models. To predict global GDP growth many economic experts have done forecasts. Following the analysis done by Capital Economics, the GDP is predicted to grow continuously with roughly 2.5% per year [39]. Therefore, this is implemented as a simple baseline for the launch traffic forecast in Fig. 12.

Table 4
Summary of model hyperparameters.

Category	Hyperparameter	Value
Architecture	Conv1D filters	64
	Conv1D kernel size	2
	Bidir. LSTM units (1st)	128
	Bidir. LSTM units (2nd)	64
	Dense units	50
	Dropout rate	0.1
Compilation	Optimizer	Adam
	Loss	Custom (Eq. (33))
Training	Max epochs	10
	Early stopping patience	10
	LR decay factor	0.5
	LR decay epoch threshold	50
Defaults	SGD learning rate	0.01
	SGD momentum	0.0
	Conv1D padding	`valid`
	LSTM activation	`tanh`

Using the GDP as an additional input for the launch traffic forecast can help improve it, but it also introduces another uncertainty. Since the exogenous data is assumed to be known also for the future years the necessity to forecast this variable arises. The accuracy of the GDP forecast can therefore influence the accuracy of the general launch traffic forecast.

4.3.3. Model architecture

The LSTM model used combines a 1D convolution layer with bidirectional LSTM layers and regularisation. It ends with dense layers for the prediction. The convolutional layer extracts local features and patterns from short subsequences. The bidirectional LSTM captures long-term dependencies in both forward and backward directions. A regularisation is introduced to prevent over fitting. The final dense layers outputs a single scalar value. As an optimizer the Adam [40], adaptive learning rate is chosen. The loss function is defined custom in Eq. (33).

$$\text{error} = y_{\text{true}} - y_{\text{pred}}$$

$$\text{loss} = \begin{cases} 5.0 \cdot \text{error}^2 & \text{if error} > 0 \\ \text{error}^2 & \text{otherwise} \end{cases}$$

$$\text{bound\_penalty} = \left[\max(0, 2 - y_{\text{pred}})\right]^2 + \left[\max(0, y_{\text{pred}} - 3000)\right]^2$$

In training the LSTM model showed a consistent underestimation of the launch values. Therefore, the loss function was defined to penalise this underestimation by scaling the squared error by 5 when the prediction is less than the true value. Additionally, it includes a soft-bound penalty to discourage predictions outside the range of 2 to 3000 objects launched per 180 days. The final loss $\mathcal{L}$ function is then defined in Eq. (33).

$$\mathcal{L} = \frac{1}{N} \sum (\text{loss} + 0.5 \cdot \text{bound\_penalty}) . \tag{33}$$

The hyperparameters of the LSTM model are demonstrated in Table 4.

4.3.4. Results

Even after implementing all of the mentioned counter measures the LSTM models do not deliver good results in both cases. Adding GDP data to the LSTM model even slightly worsens the predictions. In general, the LSTM model does not capture the up and down nature of the launch trend in recent years. The results of the tuning process are demonstrated in Fig. 13.

Compared to the historical test data (blue stars) both the LSTM model without GDP (green triangle) and with GDP (red cross) perform poorly. Both models deliver almost identical forecasts, predicting an almost steady evolution. It seems like the LSTM models tends toward the mean value of the historical number of objects launched. This could mean that the LSTM model was not able to extract a meaningful pattern. This might be due to the launches being too "random" or that there is not enough data to generalise a launch trend, thus the model is just outputting the mean value. Due to its poor performance, for the future forecast the LSTM models are not considered.

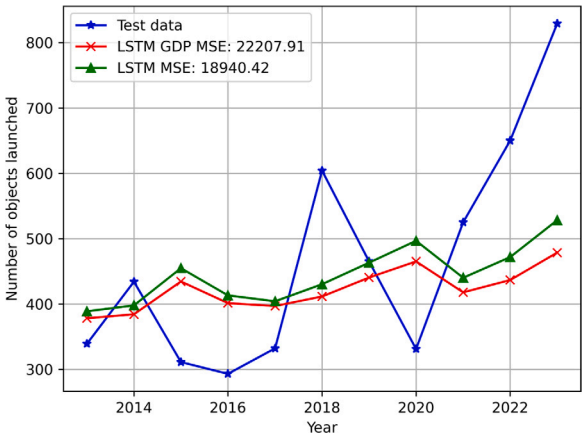

Fig. 13. The result of the LSTM tuning process. Compared to the test data both LSTM models show almost the same results. The models do not capture the fluctuation of the objects launched and instead output a mean value of the previous launch data. (For interpretation of the references to colour in this figure legend, the reader is referred to the web version of this article.)

4.4. SARIMAX

When using exogenous data for forecasting, the datasets have to span the same time horizon. In-detail data for the global GDP is available from 1990 to 2023, therefore also the historical launch data is taken from 1990–2023. To tune the respective parameters of the model and to have an idea about the quality of the forecast the data is split into a test and a train dataset. The train data spans from 1990–2015, while the test data is from 2016–2023. The test dataset will be used to evaluate the performance of the models and to help in selecting the best parameters. Before a launch model can be developed it is important to understand the historical launch data and its underlying dynamics. Particularly, the different components of the historical data are important. The data can be divided into a trend, seasonality and residuals component. To determine the seasonal factor in the historical data a Fast Fourier Transform (FFT) analysis is performed [41]. This converts the time series into a frequency domain, allowing to identify the peaks in frequency. This can be seen in Fig. 14. These peaks correspond to possible seasonal components in the time series.

A clear peak near a seasonal period of 2.3 years can be determined from Fig. 14. There is another slightly lower peak around 3.5 years. Furthermore, Fig. 14 serves as a first restriction for which parameters are of interest. After 6 years the spectrum drops significantly. The SARIMA model only takes integers as an input, therefore the best integer in the range of $s = [2, 6]$ needs to be selected. For this the data is deconstructed into its trend, seasonal and residual components (as seen in Fig. 15 for $s = 2$). Then, a reconstructed time series through the multiplicative composition of the trend and seasonal component, is compared with the original time series. In both cases the entire time period spanning from 1990–2023 is considered. The MSE between the original and the reconstructed time series can be calculated. The results are displayed in Table 5.

While Fig. 14 displays a relatively low peak at 2 years, the calculated MSE in Table 5 clearly shows the lowest MSE for $s = 2$. In the following, a seasonal period of $s = 2$ is selected. The seasonal

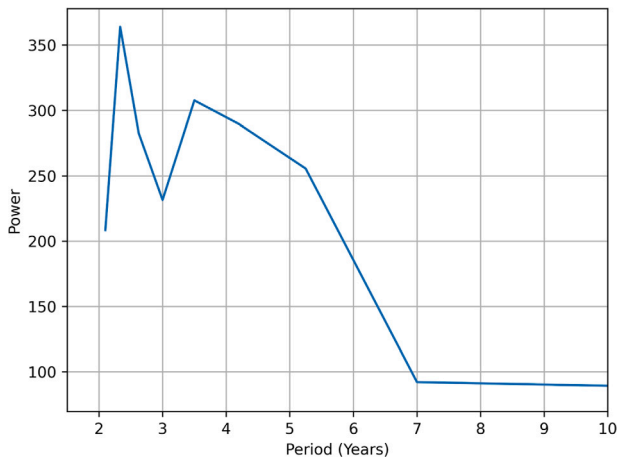

Fig. 14. The FFT power spectrum of the historical launch data transformed into a frequency domain. There is a clear peak around 2.3 years and a second pronounced peak around 3.5 years. This can serve as a guideline to choose the seasonal parameter for the SARIMA model.

Table 5
Comparison of different seasonal periods. Compared are the original time series with a reconstructed time series using the trend and seasonal components.

Period [years]	MSE
2	1777.83
3	4824.23
4	3611.13
5	4295.18
6	7069.49

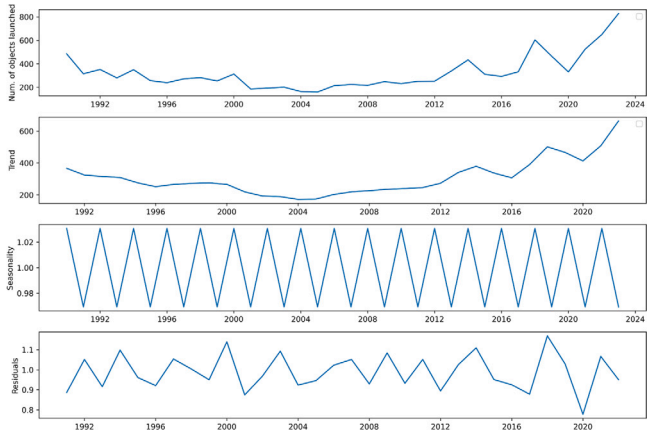

Fig. 15. The historical non-constellation launch data divided by trend, seasonality and residuals.

parameters are then set to (P, Q, D, s) = (1, 1, 1, 2) (for an explanation on the parameters see Eq. (19)). The data can be deconstructed into its trend, seasonal and residual components, as seen in Fig. 15.

The top panel shows the original time series. The second panel only shows the trend component. There is a gradual decrease from 1990 throughout the early 2000s. Then in 2010 a steady increase can be seen. The seasonal components in the third panel show a consistent oscillation pattern. The bottom panel represents the residuals, this captures outliers which are not part of the general trend. These sudden drops can be due to external factors such as the COVID pandemic in 2020. To determine the ARIMA parameters (p, q, d) (see Eq. (15)) an automated tuning process using the test/train dataset and the MSE are employed.

Table 6
The model parameters and results on the test data for SARIMA/SARIMAX. SARIMAX delivers better results, lowering the MSE by 46.27%.

Model	Parameters	MSE
SARIMA	(1,1,1,2) × (1,2,1)	15192.33
SARIMA	(1,1,1,4) × (2,2,3)	12648.84
SARIMAX with GDP	(1,1,1,4) × (2,2,3)	8157.44

Furthermore, it is also tested how using the exogenous data influences the accuracy of the forecast. For both cases the best parameters are determined separately based on the MSE. For each parameter p, q and d values between 1 and 4 are considered. The different combination of these parameters is tested via a grid search. During this process it was observed that, when using GDP data the training and future forecast showed a more stable behaviour with seasonal parameters (P, Q, D, s) = (1, 1, 1, 4). The external GDP data might influence the launches at different cycles and periods. Furthermore, the seasonal period of $s = 4$ was the second possible candidate identified in Table 5. Therefore, for the SARIMAX data a period of 4 years is set. For completeness the parameters (P, Q, D, s) = (1, 1, 1, 4) were also tested for the SARIMA model with no exogenous data. While this did improve the performance on the test data, the future forecast becomes unstable with a large oscillation. Therefore, the original seasonal period of $s = 2$ is kept for the SARIMA model. The results are then compared and demonstrated in Table 6. Additionally, in every case a Confidence Interval (CI) can be determined. The CI provides a probabilistic range in which to expect the future value. The CI is directly extracted from the statsmodels SARIMAX package [42]. They are computed assuming a standard normal distribution of the forecast errors, where the interval widens at longer horizons. The predictions of the different models including their CI are depicted in Fig. 16.

In Fig. 16 it is clearly visible that including the GDP data improves the forecast. All models were trained on the test data (orange dots) and then the predictions (red cross) were compared to the actual test launch data (blue star). In the SARIMA fitting process the model parameters and residual variances are estimated and propagated into future periods. A lower and upper bound for the CI is determined using statistical methods. Assuming a seasonal period of $s = 4$ improves the prediction also for the SARIMA model. The MSE is lowered from $\text{MSE}_{(1,1,1,2)\times(1,2,1)} = 15192.33$ to $\text{MSE}_{(1,1,1,4)\times(2,2,3)} = 12155.35$. Even with the same parameters, the model including the GDP performs better on the test data with an MSE of $\text{MSE}_{GDP:(1,1,1,4)\times(2,2,3)} = 8157.44$. Especially for the year of 2020 during the height of the COVID pandemic including the GDP data correctly predicts a drop in the launched number of objects. This improvement is reflected in the MSE, which is lowered by 46.27% in respect to the first SARIMA model and lowered by 35.49% in respect to the one with the same parameters. Even though using a seasonal period of $s = 4$ improves performance on the test data for the SARIMA model, it destabilises the future forecast. This is demonstrated in Fig. 17 (grey dashed line). The future forecast with these parameters cause an oscillation of objects launched which is not realistic. Therefore, the SARIMA model with $(1, 1, 1, 2) \times (1, 2, 1)$ still exhibits better results overall. The SARIMAX model including the GDP shows good results both for the test and the future forecast. But while the mean predictions improve, including GDP data also increases the uncertainty. This is reflected in the growing confidence interval as seen in Fig. 16.

5. Future forecast

During training the SARIMAX model with the GDP data provided the best results. When looking at the forecast for the next 25 years, the SARIMA model both with parameters $(1, 1, 1, 4) \times (2, 2, 3)$ (grey dashed line) and $(1, 1, 1, 2)\times(1, 2, 1)$ (orange diamond) and the SARIMAX model (green cross) are tested and demonstrated in Fig. 17. After determining

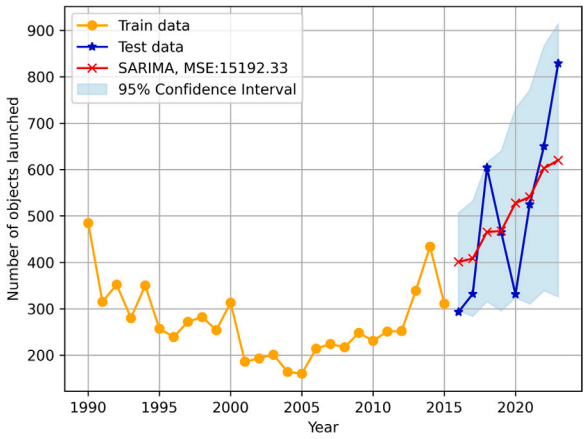

(a) Predictions using only launch data with (1,1,1,2)×(1, 2, 1). The SARIMA model predicts a steadily growing launch trend.

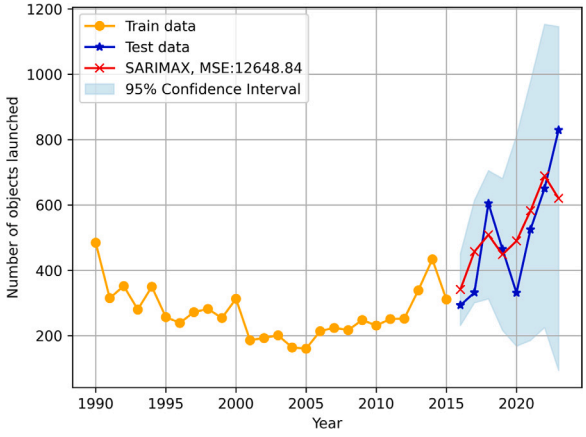

(b) Predictions using only launch data with (1,1,1,4)×(2, 2, 3). The SARIMA model predicts growing launch trend with a minimum in 2019.

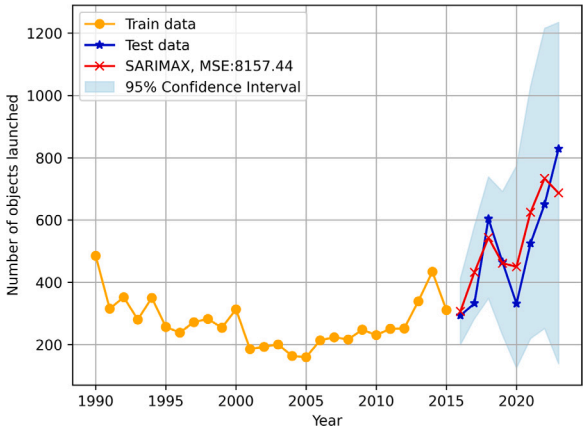

(c) Predictions using launch and GDP data with (1,1,1,4)×(2, 2, 3). The SARIMAX model correctly predicts the minimum in launches in 2020, due to having the GDP data available for this year.

Fig. 16. Comparing the predictions on test data when using economic data and not. The corresponding CI is also plotted. Including GDP data improves predictions, but also increases the uncertainty due to adding the external factor. (For interpretation of the references to colour in this figure legend, the reader is referred to the web version of this article.)

the parameters in training, the model is refitted to the entire dataset from 1990–2023 to include also the recent developments and improve the future forecast. Furthermore, two literature models are included for comparison. The first one is the classic cyclic model (pink) with a repetition of 8 years. The second one is the model presented by Velerda Escobar [8]. The number of objects launched per year is estimated using Gompertz logistic curves, defined in Eq. (34).

$$L(t) = \left[a \exp(-e^{-b-c(t-t_0)}) + d\right], \tag{34}$$

where L is the number of objects launched in the year t and t_0 is a reference year. The parameter a describes the saturation point, which is chosen based on a low (red star) and high rate (black inverted triangle) scenario before fitting the curve. The other parameters b, c and d are obtained by a fit to the data ranging between $t = 2005 - 2021$, with $t_0 = 2005$. The forecast for the next 25 years shows different behaviour depending on the model. The SARIMA model with $(1, 1, 1, 4) \times (2, 2, 3)$ shows an oscillation which is not reasonable. Instead the parameters $(1, 1, 1, 2) \times (1, 2, 1)$ deliver a more realistic steadily growing curve. Including the GDP data with the SARIMAX model predicts slightly higher launches with more variation. This variation in the launch traffic demonstrates a more realistic forecast, since the launches are not expected to keep growing every year. The Velerda Escobar model [8] demonstrates no up and down pattern and reaches its saturation point relatively quickly. The cyclic model repeats the variation in launches of the past 8 years, but predicts much lower launches per year than the other models. In summary, the SARIMAX GDP forecast shows a steady growth with realistic variations in the launches. This forecast only includes non-constellation launches. The next step is to combine one of these scenarios with the constellation launches previously determined in Section 3.

5.1. Combination of future launches

To get a full picture of the future launches both constellation and non-constellation launches should be considered. Here, three different scenarios are presented. A low rate, high rate and mean launch scenario. For the non-constellation launches an upper and lower limit of the forecast can be considered with the confidence interval. In Fig. 18 the SARIMAX GDP forecast (green cross) including the CI and upper and lower bounds (red dash) is depicted.

The further the forecast is into the future, the more the uncertainty grows. This is common for predicting long term future events and reflects that the launch activity could differ significantly depending on external conditions such as economic developments or policy changes. The SARIMAX forecast could likely be continuously improved by updating the GDP forecast according to the relevant economic events. The lower CI was clipped at the mean of lower CI between the years 2025 and 2035 = 553, since it is not realistic that the launches would go below 0. The upper and lower bound demonstrate a low and high rate scenario, which can be considered in future decision making. For the constellation launches instead the replenishment has a big influence of the number of future launches. Here, three scenarios are demonstrated. These scenarios and their assumptions are summarised in Table 7.

The low rate scenario only considers those constellations that have already started launching satellites (see Table 1) and assumes no replenishment. The 8 constellations considered are those that have not yet finished their launch plans. The mean rate scenario considers the same constellations but assumes a replenishment period of 5 years. The high rate scenario instead assumes that all 43 constellations, including those that have not started launching yet, as described in Section 3, will launch and replenish their satellites. These scenarios for both constellation and non-constellation launches can then be combined to show the full picture of the future launches in a low, mean and high rate scenario. The complete picture of the different scenarios is depicted in Fig. 19.

The low rate scenario assumes no replenishment of constellations. In 2035 all of the used constellations have reached their full size. Hereafter, only non-constellation launches are launching. For these,

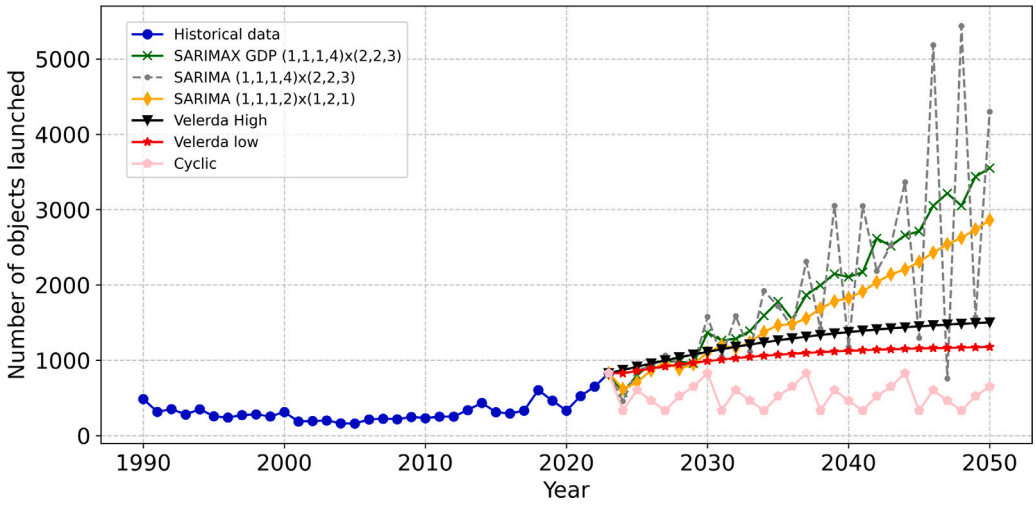

Fig. 17. The future forecast without constellations as predicted by different models. The SARIMA model with a seasonal period of s=4 delivers unrealistic results and should not be considered as a viable model. The other models predict a steadily growing launch rate. Only the SARIMAX GDP and the cyclic model demonstrate some variation in future number of objects launched instead of a smooth curve. (For interpretation of the references to colour in this figure legend, the reader is referred to the web version of this article.)

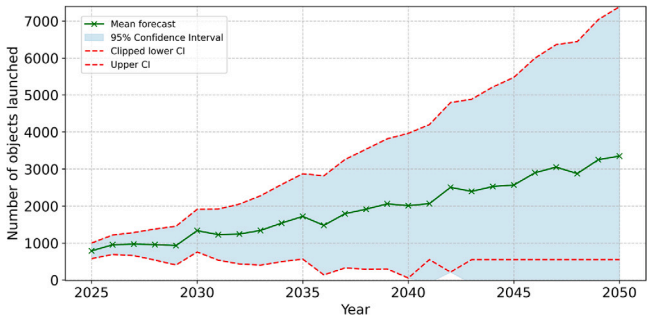

Fig. 18. The future forecast without constellations based on the SARIMAX model. The mean forecast predicts a steady growth with some slight variations. The confidence interval grows going further into the future. This can serve as an upper and lower bound for future launch forecasts. (For interpretation of the references to colour in this figure legend, the reader is referred to the web version of this article.)

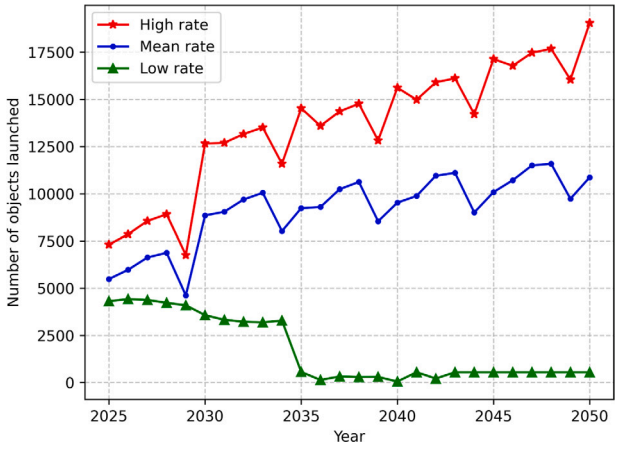

Fig. 19. The predicted launches assuming a low, mean and high rate scenario. The cyclic nature in the high and mean rate scenario are due to the 5 year replenishment period of constellations. The low rate scenario tends to the mean of the launches between 2025 to 2035. The dip in 2029 is due to all old satellites being replenished in that year.

Table 7
The different future launch scenarios and their assumptions. For the low and mean rate scenario only those constellations that have launched satellites are considered. In the low rate scenario the constellations do not replenish. The non-constellation launches are determined based on the SARIMAX forecast including GDP.

Scenario	SARIMAX	Constellations
Low rate	Lower bound of CI	8 constellations No replenishment
Mean rate	Mean forecast	8 constellations 5 year replenishment
High rate	Upper bound of CI	43 constellations 5 year replenishment

the lower bound of the clipped confidence interval from the SARIMAX forecast is used. It assumes that there will be at least 553 total launches in 2050. The mean rate scenario instead uses the same constellation launches but assumes constant replenishment and combines it with the mean of the SARIMAX forecast. In 2050 there are 10,968 predicted launches. The high rate scenario assumes all 43 constellations described in Section 3 launch and replenish their satellites. For the non-constellation launches the upper CI of the SARIMAX forecast is used. Here, in total 19421 satellites are predicted to launch in 2050. Both the high and mean rate scenario show a dip in 2029. This is due to the fact that all already launched satellites from history have been replenished at that point (see Fig. 6). To demonstrate the ratio between constellation and non-constellation launches the mean rate scenario is also plotted and split into those categories and the constellations in Fig. 20. Even assuming only those constellations that have started launching will complete their launch plans, the majority of future launches is made up of constellation launches.

6. Outlook and conclusion

This research gives a novel approach to forecast future non-constellation launch traffic based on economic influences. Both the SARIMAX model and the LSTM model were investigated. While the SARIMAX model delivered a realistic launch forecast, the LSTM model tended towards the mean of the historical data. It might be that the available data does not provide enough information to generalise from it. Possibly this could be improved by increasing model complexity or

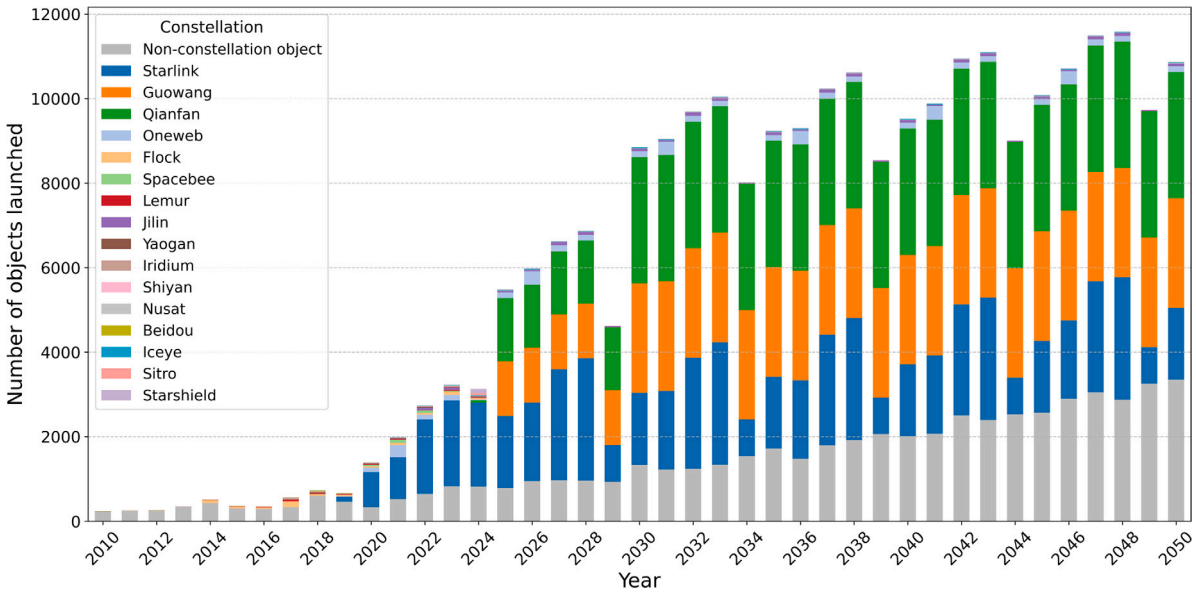

Fig. 20. This plot displays the historical launch traffic until 2024 and then the future mean rate forecast including constellations, assuming a 5 year replenishment. The launches are broken down by non-constellation and constellation launches. Of the 15 constellations plotted, 8 have not finished their launch plans and are projected into the future. Constellation launches make up the majority of the launches. In total it is projected to reach up to 11,000 launches per year. The main contributions are from Starlink, Guowang and Qianfan.

providing more features for the LSTM model. With the SARIMA model instead, the inclusion of an economic factor such as the global GDP greatly improved the prediction. Even though the *PCC* of 0.57 showed only a moderate linear correlation, the forecast already improved significantly. This could further be enhanced by researching other more strongly correlated economic factors such as space investment. But here, the issue of public data availability creates a challenge. Furthermore, it is to be considered that with the addition of this exogenous data another source of uncertainty is introduced. Due to the nature of the time series methods the exogenous data has to be available for the entire forecasting horizon. Hence, the need arises to predict not only the future launches, but also the future GDP. The accuracy of this GDP forecast will influence the accuracy of the launch prediction. This growing uncertainty is demonstrated with the growing confidence intervals seen in Fig. 18. Nonetheless, the forecast can serve as a valuable reference point for what the future launch landscape could look like. The provided confidence interval can serve as an upper and lower bound for a low and high launch scenario. In practice, the model should be updated based on a yearly basis with the most recent launch and GDP data to further improve predictions. The constellation launches were predicted based on publicly available statements of intent by companies. Taking these into account shows that the vast majority of future launches will come from satellite constellations. With this bulk of constellation launches, the contribution of the non-constellation launches is secondary. To note is that the constellation launches are predicted assuming no sudden changes such as a market collapse or regulatory restrictions. An analysis of historical data has shown that even during unstable periods such as the Covid pandemic, constellation launch rates were not affected. Even assuming that only those constellations that have already started launching will complete their plans, the future constellation launches make up over 90% of the planned launches. This raises questions about orbital capacity and the impact that such a volume of launches could have on the space environment as a whole. If regulatory restrictions are placed on constellation launches, the number of non-constellation objects carry more weight again. In future works this impact will be investigated by using the forecast as an input for a space debris environment model. In particular, it will be interfaced with a long term debris evolution environment model to study the sensitivity of the environment to launch traffic and the exponential increase of debris. For this application the distribution of the launches in orbital elements, mass, area and object category will be determined. For constellation launches this will be done by looking at the company's plans. For non-constellation launches instead a historical distribution can be built from the DISCOS data using techniques such as Gaussian-Mixture Models, Machine Learning or random sampling.

CRediT authorship contribution statement

Wiebke Retagne: Writing – original draft, Visualization, Validation, Software, Methodology, Investigation, Formal analysis, Data curation, Conceptualization. **Camilla Colombo:** Writing – review & editing, Supervision, Project administration, Funding acquisition.

Declaration of competing interest

The authors declare that they have no known competing financial interests or personal relationships that could have appeared to influence the work reported in this paper.

Acknowledgements

This research received funding from the European Research Council (ERC) under the European Union's Horizon Europe research and innovation program as part of the GREEN SPECIES project (Grant agreement No - 101089265). We acknowledge ESA's efforts to maintain and operate the DISCOS database with its Application Programming Interfaces (APIs). We would also like to thank Erik Kulu for the maintenance of the NewSpace Index website. Lastly, we would like to thank the reviewers for their valuable feedback, which helped increase the quality of this work.

Appendix. Constellation tables [2]

See Table A.1.

Table A.1

Organization	First launch	Form factor	Field	Planned	In_Sample
Hongqing Technology	2025	?	Internet	10000	FALSE
Hanwha Systems	*2025*	*?*	*Internet, 6G*	*2000*	*TRUE*
Constellation Technologies	2026	Satellite	Internet	1500	FALSE
Logos Space	2027	?	Internet	1092	FALSE
UNIO	2025	Smallsat	Internet	1000	FALSE
Mangata Networks	2025	Satellite	Internet, 5G	791	FALSE
Lumen Orbit	*2025*	*Microsat*	*Space Data Center*	*300*	*TRUE*
Rivada (OuterNET)	2026	Smallsat, ?	Internet	300	FALSE
SpaceRISE (IRIS2)	2029	?	Internet, 5G	290	FALSE
Startical	*2025*	*Smallsat, CubeSat*	*VHF Radio Communications*	*288*	*TRUE*
SpinLaunch (Meridian Space)	2026	Microsat	Internet	280	FALSE
Marble Imaging	2026	Microsat	Earth Observation, Optical	200	FALSE
Astrome	*2025*	*Microsat*	*Internet*	*198*	*TRUE*
Telesat (Lightspeed)	2026	Smallsat	Internet, Orbital Data Relay	198	FALSE
Inmarsat (ORCHESTRA)	2025	Satellite	Internet, Direct-to-Cell, Direct	175	FALSE
EnduroSat (Balkan)	*2025*	*CubeSat?*	*Earth Observation*	*120*	*TRUE*
Alya Space (Alya 1)	*2025*	*8U, Microsat*	*Earth Observation*	*108*	*TRUE*
Xenesis (Intercessor)	2026	?	Orbital Data Relay	98	FALSE
Ingenu (AFNIO)	*2025*	*Microsat, ?*	*IoT / M2M*	*72*	*TRUE*
Bluelink Satcom	*2025*	*Microsat, ?*	*IoT / M2M, Bluetooth*	*72*	*TRUE*
Reflect Orbital	*2025*	*?*	*Wireless Energy Supply*	*57*	*TRUE*
Muon Space	*2025*	*Microsat*	*Earth Observation*	*50*	*TRUE*
Climavision	2025	?	Weather	50	FALSE
Globalstar (Third Generation)	2027	Smallsat, ?	Internet, IoT / M2M	50	FALSE
Argotec	*2025*	*Microsat*	*Earth Observation*	*40*	*TRUE*
Tianjin Satcom (36 Tiangang)	*2025*	*?*	*SAR, Earth Observation*	*36*	*TRUE*
EOI Space (Stingray)	2025	Smallsat	Earth Observation, Optical, VL	30	FALSE
Volta (LightGrid)	2026	?	Wireless Energy Supply	30	FALSE
EchoStar (Lyra)	*2025*	*Microsat*	*IoT / M2M*	*28*	*TRUE*
Mission Space	*2025*	*Hosted, 3U, 6U*	*Space Weather*	*24*	*TRUE*

(continued on next page)

Table A.1 (*continued*).

Organization	First launch	Form factor	Field	Planned	In_Sample
Absolut Sensing (GESat)	*2025*	*16U*	*Emissions Monitoring*	*24*	*TRUE*
Almagest	*2025*	*?*	*Orbital Data Relay*	*24*	*TRUE*
GALAXIA Mission Systems	2025	CubeSat	Earth Observation	24	FALSE
Scepter	2025	Microsat	Emissions Monitoring	24	FALSE
NIBE Space	*2025*	*Smallsat*	*Earth Observation*	*23*	*TRUE*
NUVIEW	*2025*	*?*	*Earth Observation*	*20*	*TRUE*
Spiral Blue	2027	Microsat, ?	3D Imaging, LIDAR	20	FALSE
LUMIR	2026	Microsat, ?	SAR	18	FALSE
Globalstar	2025	Smallsat, ?	Internet, IoT / M2M	17	FALSE
4pi Lab (EPiC)	*2025*	*?*	*Earth Observation*	*16*	*TRUE*
Methera	*2025*	*Smallsat*	*Internet, SSA*	*16*	*TRUE*
LusoSpace	*2025*	*8U, 3U*	*VDES (AIS 2.0), AIS*	*12*	*TRUE*
Vyoma Space (Flamingo)	*2025*	*Microsat, ?*	*SSA*	*12*	*TRUE*
Laser Light (HALO)	*2025*	*Smallsat*	*Laser Communications*	*12*	*TRUE*
Cloud Constellation	*2025*	*Smallsat*	*Data Storage*	*12*	*TRUE*
AIRMO	*2025*	*CubeSat?*	*Emissions Monitoring*	*12*	*TRUE*
HySpecIQ (HySpec)	2025	Satellite	Earth Observation	12	FALSE
AAC Clyde Space	*2025*	*16U*	*Earth Observation*	*10*	*TRUE*
EarthDaily Analytics	2025	Microsat	Earth Observation, Optical	10	FALSE
Orbitworks (Altair)	2026	Smallsat	Earth Observation	10	FALSE
Metrea (XR)	*2025*	*Microsat, ?*	*SAR, Earth Observation*	*8*	*TRUE*
4iG (HULEO)	2028	?	Earth Observation	8	FALSE
Albedo Space (Clarity)	*2025*	*Smallsat, ?*	*Earth Observation, Optical*	*6*	*TRUE*
Amini	*2025*	*?*	*Earth Observation, Optical*	*6*	*TRUE*
HyperSat	2025	Smallsat	Earth Observation	6	FALSE
Lonestar	2027	Hosted, ?	Data Storage	6	FALSE
TALOS (ICARUS)	*2025*	*CubeSat*	*IoT / M2M*	*5*	*TRUE*
SatSure (KaleidEO)	*2025*	*Microsat*	*Earth Observation, Optical*	*4*	*TRUE*
Rapid Cubes	*2025*	*16U*	*IoT / M2M*	*4*	*TRUE*
BAE Systems (Azalea)	*2025*	*Smallsat*	*Earth Observation, SAR*	*4*	*TRUE*
Instinct	2025	CubeSat?	PNT	4	FALSE
Kongsberg (N3X, ARVAKER)	*2025*	*Microsat*	*AIS*	*3*	*TRUE*
Iota Technology	2025	4U	Geomagnetic	3	FALSE
LatConnect 60 (SWIRSAT)	2026	Microsat	Earth Observation, Optical	3	FALSE
KappaZeta (3D-SAR)	2028	Smallsat, ?	SAR, 3D Imaging	3	FALSE

References

[1] T. Pultarova, SpaceX Starlink satellites made 50,000 collision-avoidance maneuvers in the past 6 months: What does that mean for space safety? Space.Com (2024) URL https://www.space.com/spacex-starlink-50000-collision-avoidance-maneuvers-space-safety. (Accessed 15 July 2025).

[2] E. Kulu, NewSpace index, 2025, https://www.newspace.im/. (Accessed 29 April 2025).

[3] H. Klinkrad, Space debris: Models and risk analysis, in: Springer Praxis Books, Springer, Berlin, Heidelberg, 2006, http://dx.doi.org/10.1007/3-540-37674-7.

[4] P. Krisko, N. Johnson, J. Opiela, EVOLVE 4.0 orbital debris mitigation studies, Adv. Space Res. 28 (9) (2001) 1385–1390.

[5] H. Lewis, Understanding long-term orbital debris population dynamics, J. Space Saf. Eng. 7 (3) (2020) 164–170.

[6] J.-C. Liou, N. Johnson, N. Hill, Controlling the growth of future LEO debris populations with active debris removal, Acta Astronaut. 66 (5–6) (2010) 648–653.

[7] J. Dolado-Perez, B. Revelin, R. Di-Costanzo, Sensitivity analysis of the long-term evolution of the space debris population in LEO, J. Space Saf. Eng. 2 (1) (2015) 12–22.

[8] J.C. Velerda Escobar, Continuum Approach for the Modelling of Debris Population and Launch Traffic in Low Earth Orbit (Master's thesis), Politecnico di Milano, School of Industrial and Information Engineering, 2022, Supervisor: C. Colombo, Co-supervisor: L. Giudici.

[9] C.J. Wilson, M. Vasile, J. Feng, K. McNally, A. Antón, F. Letizia, Modelling future launch traffic and its effect on the LEO operational environment, in: AIAA SciTech 2024 Forum, AIAA, American Institute of Aeronautics and Astronautics, Orlando, Florida, United States, 2024, http://dx.doi.org/10.2514/6.2024-181, Peer-reviewed, accepted author manuscript.

[10] M. Lifson, A. Baset, G. Cates, B. Chen, A. Connor, C. Coursey, G. Henning, M. Miyamoto, G.E. Peterson, B. Weeden, G. Williams, I. Brownhall, M. Burgess, M. Holzinger, D. Kaffine, M. Moretto, A. Rao, Development of reference scenarios and supporting inputs for space environment modeling, in: Proceedings of the Advanced Maui Optical and Space Surveillance Technologies Conference, AMOS, The Aerospace Corporation, 2024, Copyright ©2024 Advanced Maui Optical and Space Surveillance Technologies Conference (AMOS) – www.amostech.com.

[11] C. Wiedemann, M. Oswald, J. Bendisch, H. Sdunnus, P. Vörsmann, Cost and benefit analysis of space debris mitigation measures, Acta Astronaut. 55 (3) (2004) 311–324, http://dx.doi.org/10.1016/j.actaastro.2004.05.011, New Opportunities for Space. Selected Proceedings of the 54th International Astronautical Federation Congress, URL https://www.sciencedirect.com/science/article/pii/S0094576504001547.

[12] A. Rao, F. Letizia, A coupled econometric model of the orbital environment, in: Proceedings of the 8th European Conference on Space Debris, ESA Space Debris Office, Darmstadt, Germany, 2021, URL https://conference.sdo.esoc.esa.int/proceedings/sdc8/paper/206/SDC8-paper206.pdf.

[13] M. Rusconi, C. Colombo, A model-based control framework for space debris management, Acta Astronaut. 240 (2026) 384–397, http://dx.doi.org/10.1016/j.actaastro.2025.12.018, URL https://www.sciencedirect.com/science/article/pii/S0094576525008835.

[14] M. Kunz, S. Birr, M. Raslan, L. Ma, Z. Li, A. Gouttes, M. Koren, T. Naghibi, J. Stephan, M. Bulycheva, M. Grzeschik, A. Kekić, M. Narodovitch, K. Rasul, J. Sieber, T. Januschowski, Deep learning based forecasting: a case study from the online fashion industry, 2023, arXiv:2305.14406, URL https://arxiv.org/abs/2305.14406.

[15] L. Rubio, A.J. Gutiérrez-Rodríguez, M.G. Forero, EBITDA index prediction using exponential smoothing and ARIMA model, Mathematics 9 (20) (2021) http://dx.

doi.org/10.3390/math9202538, URL https://www.mdpi.com/2227-7390/9/20/2538.
[16] T. Munir, M. Khan, S.A. Cheema, F. Khan, A. Usmani, M. Nazir, Time series analysis and short-term forecasting of monkeypox outbreak trends in the 10 major affected countries, BMC Infect. Dis. 24 (1) (2024) 16, http://dx.doi.org/10.1186/s12879-023-08879-5.
[17] R.A. Angryk, P.C. Martens, B. Aydin, M. Suleiman, D. Kempton, J.C. Allred, C. Angryk, K.D. Borne, Multivariate time series dataset for space weather data analytics, Sci. Data 7 (2020) 227, http://dx.doi.org/10.1038/s41597-020-0548-x.
[18] Y. Chen, K. Wang, Prediction of satellite time series data based on long short term memory-autoregressive integrated moving average model (LSTM-ARIMA), in: 2019 IEEE 4th International Conference on Signal and Image Processing, ICSIP, 2019, pp. 308–312, http://dx.doi.org/10.1109/SIPROCESS.2019.8868350.
[19] E. Stevenson, V. Rodriguez-Fernandez, H. Urrutxua, V. Morand, D. Camacho, Self-supervised machine learning based approach to orbit modelling applied to space traffic management, 2023, arXiv:2312.06854, URL https://arxiv.org/abs/2312.06854.
[20] W. Retagne, E. Boccolari, C. Colombo, Launch traffic model for space debris evolution based on historical data and economic forecasting methods, in: 9th European Conference on Space Debris, ESA Space Debris Office, Bonn, Germany, 2025, URL https://conference.sdo.esoc.esa.int/proceedings/sdc9/paper/195.
[21] European Space Agency, DISCOS: Database and Information System Characterising Objects in Space, 2024, https://discosweb.esoc.esa.int/. (Accessed 21 July 2025).
[22] European Space Agency (ESA), Report on the Space Economy: The Space Economy in 2024, Technical report, European Space Agency, Paris, France, 2025, Annual update on global and European space industry trends, URL https://space-economy.esa.int/documents/tJMabTj61KkdGVOtF6SKw6wGSxicen6ajUWamCG3.pdf.
[23] R.J. Hyndman, G. Athanasopoulos, Forecasting: Principles and Practice, third ed., OTexts, Melbourne, Australia, 2021, URL https://otexts.com/fpp3. (Accessed 10 July 2025).
[24] S. Hochreiter, J. Schmidhuber, Long short-term memory, Neural Comput. 9 (1997) 1735–1780, http://dx.doi.org/10.1162/neco.1997.9.8.1735.
[25] M. Kolambe, Forecasting the future: A comprehensive review of time series prediction techniques, J. Electr. Syst. 20 (2024) 575–586, http://dx.doi.org/10.52783/jes.1478.
[26] M.C.A. Picoli, G. Camara, I. Sanches, R. Simões, A. Carvalho, A. Maciel, A. Coutinho, J. Esquerdo, J. Antunes, R.A. Begotti, D. Arvor, C. Almeida, Big earth observation time series analysis for monitoring Brazilian agriculture, ISPRS J. Photogramm. Remote Sens. 145 (2018) 328–339, http://dx.doi.org/10.1016/j.isprsjprs.2018.08.007, SI: Latin America Issue, URL https://www.sciencedirect.com/science/article/pii/S0924271618302260.
[27] P. Thaker, A. Desai, P. Panchal, D. Sutaria, M. Shah, M. Prajapati, Evaluating AI approaches for space weather prediction: Strengthening satellite resilience and technology systems, Space Habitat. 1 (3) (2025) 100032, http://dx.doi.org/10.1016/j.spaceh.2025.100032, URL https://www.sciencedirect.com/science/article/pii/S2950616625000300.
[28] G.E.P. Box, G.M. Jenkins, Time Series Analysis: Forecasting and Control, Holden-Day, San Francisco, 1970.
[29] A. Zhang, Z.C. Lipton, M. Li, A.J. Smola, Long short-term memory (LSTM), 2024, https://d2l.ai/chapter_recurrent-modern/lstm.html. (Accessed 29 September 2025).
[30] E. Kulu, SatRev — Satellite constellation, 2025, https://www.newspace.im/constellations/satrev. (Accessed 09 July 2025); published approximately January 2025.
[31] E. Kulu, Hongqing satellite constellation, 2026, https://www.newspace.im/constellations/hongqing-technology. (Accessed 05 March 2026); published approximately January 2025.
[32] Future oneweb launches, 2025, https://www.telecoms.com/satellite/eutelsat-to-launch-another-100-oneweb-satellites. (Accessed 12 June 2025).
[33] M. Wall, President obama's space legacy: Mars, private spaceflight and more, Space.Com (2017) URL https://www.space.com/35394-president-obama-spaceflight-exploration-legacy.html. (Accessed 23 July 2025).
[34] N.V. Patel, How the Space Industry Adjusted to the Coronavirus Pandemic, Tech. rep., 2020, URL https://www.technologyreview.com/2020/06/10/1003101/how-space-industry-nasa-adjusted-coronavirus-pandemic/. (Accessed 05 March 2026).
[35] S. Kacapyr, Cracker-sized satellites demonstrate new space tech, Cornell Chron. (2019) URL https://news.cornell.edu/stories/2019/06/cracker-sized-satellites-demonstrate-new-space-tech. (Accessed 05 June 2025).
[36] World Bank, J. Bolt, J.L. van Zanden, A. Maddison, Global GDP over the long run – Maddison Database, Maddison Project Database, World Bank – In constant international-. Historical data, 2025, https://ourworldindata.org/grapher/global-gdp-over-the-long-run, Data compiled from World Bank ("World Development Indicators"), Maddison Project Database 2023, and Maddison Database 2010. Major processing by Our World in Data. Retrieved May 12, 2025.
[37] P. Sedgwick, Pearson's correlation coefficient, BMJ 345 (2012) http://dx.doi.org/10.1136/bmj.e4483, e4483–e4483.
[38] S&P Global Market Intelligence, US monthly GDP (MGDP) index, 2025, Online product page and data releases, Monthly indicator of real aggregate output, conceptually consistent with BEA GDP; current index published as of June 2, 2025, URL https://www.spglobal.com/market-intelligence/en/solutions/products/us-monthly-gdp-index.
[39] Capital Economics, What will the global economy look like in 2050?, 2024, https://www.capitaleconomics.com/what-will-global-economy-look-2050. (Accessed 13 July 2025).
[40] D.P. Kingma, J. Ba, Adam: A method for stochastic optimization, 2017, arXiv:1412.6980, URL https://arxiv.org/abs/1412.6980.
[41] H. Musbah, M. El-Hawary, H. Aly, Identifying seasonality in time series by applying fast Fourier transform, in: 2019 IEEE Electrical Power and Energy Conference, EPEC, 2019, pp. 1–4, http://dx.doi.org/10.1109/EPEC47565.2019.9074776.
[42] Statsmodels Developers, Statsmodels: Statistics in python — Documentation (version 0.8.0), 2017, https://www.statsmodels.org/0.8.0/index.html. (Accessed 05 March 2026).